文章编号：1001-9014(2023)06-0772-08

DOI:10.11972/j.issn.1001-9014.2023.06.010

Design of the integrated interaction circuits for a 200-kW Ka-band klystron with two output ports

BI Liang-Jie, JIANG Xin-Yu, LI Hai-Long*, WANG Bin, MENG Lin, YIN Yong

(School of Electronic Science and Engineering, University of Electronic Science and Technology of China, Chengdu 610054, China)

Abstract: In this paper, an efficient resonant circuit based on integrated interaction units is proposed to improve the beam-wave interaction for increasing the peak power of a Ka-band klystron to 200 kW. The integrated-unit circuit is designed with connecting two or several single-beam-wave interaction units across the cross section (each of which is typically used in a conventional single-beam klystron) based on the cascaded field structure in the rectangular gap waveguide with specific fusion boundary conditions. For the input cavity, two interaction units have been efficiently integrated to obtain the optimal absorption efficiency with the constant input power at ~35 GHz, through optimizing both the beam-loading parameters and cavity parameters. The output cavity has been 1) designed with two output ports for balancing the effect of the power extraction on the integrated circuit, and 2) optimized to deliver 200-kW peak power through injecting two pre-modulated beams. The overall interaction circuit of a Ka-band klystron is accordingly designed to produce the peak power of 202.9-kW with the efficiency of 40.2% and the maximum gain of 47 dB using particle-in-cell (PIC) simulations, when the two beams with the voltage of 45 kV and every current of 5.6 A are used to drive the klystron.

Key words: klystrons, distributed beam, integrated interaction unit, high power millimeter-wave sources, vacuum electronics

一种具有双输出端口的200-kW Ka波段速调管的集成互作用电路设计

毕亮杰，蒋欣宇，李海龙*，王 彬，蒙 林，殷 勇

(电子科技大学 电子科学与工程学院，四川 成都 610054)

摘要：文章提出了一种基于集成互作用单元的高效谐振电路，以改善注波互作用，将Ka波段速调管的峰值功率提高到200 kW。被集成的单元电路设计是基于矩形间隙波导中级联的场结构，通过特定边界条件的融合，将两个或多个单注-波互作用单元横向连接在一起(每个单元通常用于传统的单注速调管)。针对输入腔，通过优化注加载参数和腔体参数将两个互作用单元有效地整合在一起，以获得~35 GHz恒定输入功率下的最佳吸收效率。输出腔1)设计有两个输出端口，以平衡功率提取对集成互作用电路的影响；2)通过优化两个预调制的电子束得到200-kW的峰值功率。在注电压为45 kV、单个注电流为5.6 A的条件下，通过粒子模拟(PIC)，所设计的Ka波段速调管的整体互作用电路能够产生202.9-kW的峰值功率，效率为40.2%，增益最大达到47 dB。

关 键 词：速调管；分布式电子束；集成互作用单元；高功率毫米波源；真空电子学

中图分类号：TN122　　**文献标识码**：A

Introduction

Klystrons, are widely used microwave amplifiers based on the vacuum electronic technology [1,2]. Such amplifiers provide efficient amplification with a high level of output power generally not achievable by other de-

Received date: 2023-02-03, **revised date**: 2023-06-01　　**收稿日期**：2023-02-03，**修回日期**：2023-06-01

Foundation items: Supported by the Natural Science Foundation of Sichuan Province (2023NSFSC1376)

Biography: BI Liang-Jie (1990-), Male, Born in Yuanping, Shanxi, China. Research interests include millimeter waves and THz vacuum electronic devices, high power microwave technique and their applications. E-mail: blj@uestc.edu.cn

* **Corresponding author**: E-mail: lihailong@uestc.edu.cn

vices, based on their two distinguishing features [3] that: 1) the microwave-generating interactions in these devices take place in resonant cavities at discrete locations along the beam, and 2) the drift tube connecting the cavities is designed so that the electromagnetic wave propagation at the operating frequency is cut off between the cavities; without electromagnetic couplings between cavities, they are coupled only by the bunched beam, which drifts from one cavity to the next. Today, it is of great interest in developing low voltage, efficient, high power klystrons at Ka-band, due to numerous applications in ground, air, or aerospace systems [4].

For single-beam klystrons, Communications & Power Industries (CPI) have produced Ka-band extended interaction klystrons with the 1-kW continuous wave (CW) or the 3.5-kW pulsed power [5]. The Chinese Academy of Sciences has developed a Ka-band extended interaction klystron (EIK) with the maximum output power of 20 kW and the efficiency of 24%[6], which was achieved by using a higher compression electron gun with the perveance of 0.745 μP (25.5 kV/3.1 A). The peak power of a Ka-band klystron has been increased to up to 100 kW [7] in the design level, for example, of a simulated case with an electron beam with the voltage of 40 kV and 6 A (0.75 μP).

To increase the power to over 100 kW and higher level, however, the single-beam-wave interaction used in conventional single-beam klystrons is difficult to generate such high power because the beam power is limited by the small beam current density at low voltage (lower than 50 kV). Accordingly, the efficient beam power transferred to millimeter waves is insufficient with a single interaction circuit in single-beam klystrons. To explain clearly the basic idea in this paper, we regard the single interaction circuit as a typical model of one beam-wave interaction unit.

For the high power and high efficiency specifications, the efficient combination of several beam-wave interaction units is fundamental to the design of a klystron or EIK, since it can be used not only for matching with distributed electron beams, but also for forming an improved interaction mechanism through promoting and achieving each other between the units. Every interaction unit follows a typical single-beam-wave interaction supporting conventional klystrons.

There have been several schemes suggested to integrate two or more interaction units, such as 1) the double-beam circuits [8-12] with ridge-loaded structures or other waveguide structures, and 2) multi-beam circuits with coaxial structures [13-18]. These schemes have shown efficient interaction capabilities through combining two or several units with different ways. For example, the scheme in Ref. [8] uses the ridge-loaded structure in the typical ladder-type structure to integrate two interaction units, which is supported by the overlapping mode of TM_{11} and TM_{21}, and aimed to achieve a breakthrough for EIKs at 220 GHz. Differently, the scheme in Ref. [9] distributes two coplanar beams along the cross section of an identical gap based on the TM_{21} mode, which behaves as using a rectangular gap to directly integrate two interaction units with the opposite phases of the electric field respectively. It aims to obtain kW-level output power for a 220-GHz EIK. Last but not least, the scheme 2) depends on the coaxial structure with multiple beams that becomes a good selection for integrating more than two interaction units and accordingly generating high power millimeter wave radiation.

In fact, the development of Ka-band klystrons toward over 100 kW needs not only integrate efficient interaction units, but also efficient power extractions for improving the power capacity and the circuit efficiency. This paper provides a new method of integrating two interaction units for producing two times the current level (100 kW). The integrated two units are supported by the in-phase electric field and on this basis, we propose a Ka-band klystron with two output ports for generating 200-kW peak power. The evolution from an interaction unit to the new circuit integrating two units is analyzed from the physical mechanism. The basic designs of the input cavity and output cavity with two output ports are shown to support the proposed Ka-band klystron amplifier. Finally, the beam-wave interaction capability of the amplifier is simulated to demonstrate the effectiveness of the amplifier operation.

1 Basic idea of the integrated-unit circuit

A beam-wave interaction unit is defined as a single-gap resonant cavity usually used in single-beam klystrons. Here, its basic structure is a rectangular gap with its narrow side being placed along the *z*-direction. Figure 1(a) shows the cross section of a typical single-gap resonant cavity usually used in klystrons. The circle in the central location represents an electron beam tunnel passing through the narrow side. It is as a result of Eigenmode calculations that the TM_{11} mode is resonated with the wavelength of $\lambda_{g0}/2$. λ_{g0} is the standing wavelength of the rectangular gap along the *x*-direction.

Two or three such units can be directly arranged along the x-direction, as shown in Figs. 1(b) and 1(c). This lies in the fact that the original electric boundary conditions at the ends along the *x*-direction can be coincided to form a common, inherent boundary condition between the two adjacent units. Based on such inherent boundary conditions, the integrated two and three units resonate with the TM_{12} mode and the TM_{13} mode, respectively. The E_z field with the wavelength of $\lambda_{g0}/2$ is copied to form two and three such fields with each of them distributing as the same $\lambda_{g0}/2$. The copied E_z field in the integrated two units has an opposite phase between the adjacent units. The frequency of the integrated units is almost the same as that of the single unit, as shown in Fig. 1(a). This lays the foundation for the efficient integration of the units directly connected as the way shown in Figs. 1(b) and 1(c).

It should be noted from the case shown in Fig. 1(b) that 1) the two electron beams would experience the E_z fields with opposite phases, 2) the power extraction from

any one of the two units would cause structural asymmetry, and 3) the structure for directly extracting the power from either gap in the two units would be close to the corresponding electron beam, which may affect the field uniformity and the beam-wave interaction. The point 1) would be changed in the case shown in Fig. 1(c), because the E_z fields distributed on both sides of the units have the same phase when interacting with two beams.

However, this case still faces the same points as 2) and 3). With the motivation for eliminating these two points, we consider designing two identical coupling cavities to locate on both sides of the middle unit along the *y*-direction, and choosing to place no electron beam in the middle unit. Then the output structure of power extraction can be designed upon one of the coupling cavities or upon both, as shown in Fig. 2. Such an output structure is relatively far from the two electron beams and two such structures are symmetrically located on both sides of the symmetrical coupling cavities. The whole integrated cavity maintains good geometric symmetry and accordingly, reduces the field nonuniformity caused by the loading of the output structure.

According to the basic idea above, the directly connected three-unit cavity shown in Fig. 1(c) evolves into the integrated two-unit cavity shown in Fig. 1(d). To maintain the same resonant frequency of two cavities, the E_z fields with three uniform wavelengths of $\lambda_{g0}/2$ (Fig. 1(c)) are transferred into the new E_z fields with three different wavelengths of $\lambda_{g2}/2$, $\lambda_{g1}/2$, and $\lambda_{g0}/2$ [19-21] (Fig. 1(d)), respectively.

2 Analysis of the input cavity with two beam loading

The structural symmetry of the integrated units determines that the two units have the same E_z field distribution. Then the beam loading in the two units of the integrated cavity would exert the same effect on the electromagnetic characteristics of the cavity. For a beam-loaded cavity, the beam parameters, and the cavity parameters should be selected and optimized in both directions to obtain the optimal modulation and absorption of the input power at a given frequency. This depends on the matching between the beam perveance and the field distribution across the gap of the unit. It is consequently important to select the gap width of every unit for determining the shape factor of the E_z field, which makes the g_e value larger than 0 or close to 0 within the designed beam perveance.

Here, the perveance of a single electron beam driving one unit is limited by the constant beam power of ~ 500 kW with the efficiency of 40 % and the peak microwave power of 200 kW in consideration. The marks 1, 2, 3, 4, 5, 6, 7, 8 represent the beam voltages of 30 kV, 33 kV, 36 kV, 39 kV, 42 kV, 45 kV, 48 kV, 51 kV, with the currents of 8.4 A, 7.64 A, 7 A, 6.46 A, 6 A, 5.6 A, 5.25 A, and 4.94 A, respectively. Through dozens of optimizations in simulations, the gap width is chosen as 0.9 mm, which makes g_e larger than 0 within the full range of the perveance, as shown in Fig. 3. The corresponding E_z field distribution of the operating mode of the integrated cavity is shown in Fig. 4(a). It should be noted that 1) the value of effective characteristic impedance (M^2R/Q) is the same for the two units because the E_z field distribution in them is the same, and 2) the M^2R/Q is increased to the maximum value as the voltage increases to be within 40-50 kV, which is the desired voltage range for the design work of the klystron. The elec-

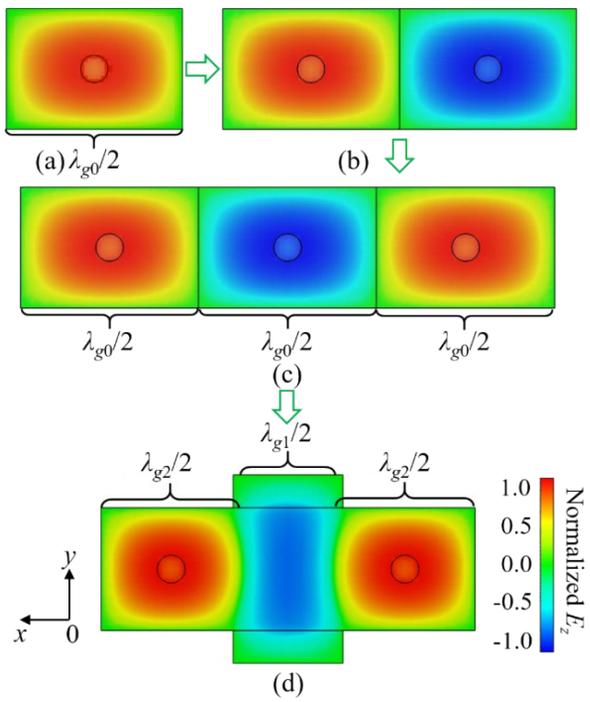

Fig. 1 (a) The conventional interaction unit with the E_z field across the $\lambda_{g0}/2$ length, (b) two such units connected along the *x*-direction to form an integrated-two-unit circuit, (c) the integrated-three-unit circuit formed by connecting three such units along the *x*-direction, and (d) the proposed integrated-two-unit circuit with specific coupling cavities for power extraction
图1 (a)具有$\lambda_{g0}/2$长度分布的E_z场的传统互作用单元电路,(b)沿x轴方向级联的两个该单元电路形成的一个两单元集成互作用电路,(c)由沿x轴方向级联的三个该单元电路形成的三单元集成互作用电路,和(d)用于功率提取的具有特定耦合腔的两单元集成电路

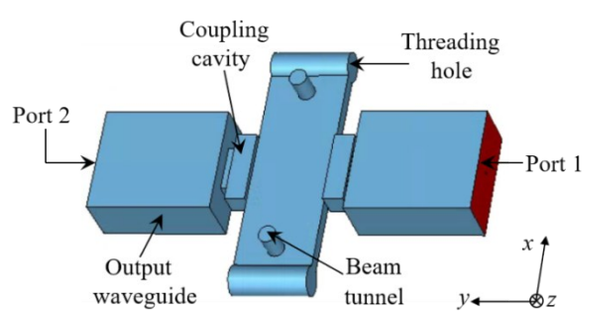

Fig. 2 The schematic drawing of the integrated-two-unit circuit with two output ports located on both sides of the two symmetrical coupling cavities
图2 两个输出端口位于两个对称耦合腔两侧的两单元集成电路的示意图

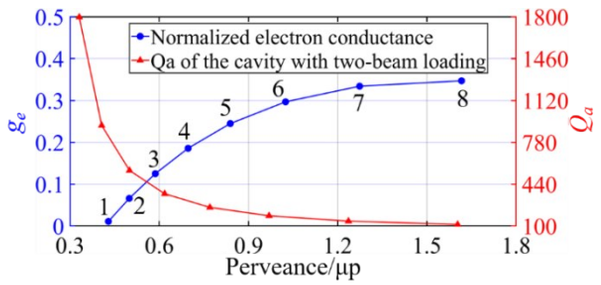

Fig. 3　The effect of the beam perveance on g_e and Q_a
图3　电子束导流系数对电子电导g_e和Q_a的影响

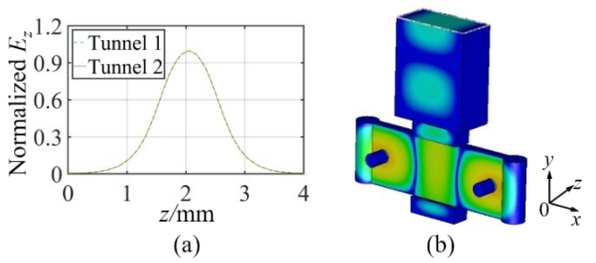

Fig. 4　(a) The E_z field along the axis of tunnel 1 and 2, and (b) the three-dimensional (3-D) model of the input cavity with the 3-D distribution of the E_z field
图4　(a)沿电子束通道1和2轴线分布的E_z场和(b)具有E_z场的三维分布的输入腔三维(3-D)模型

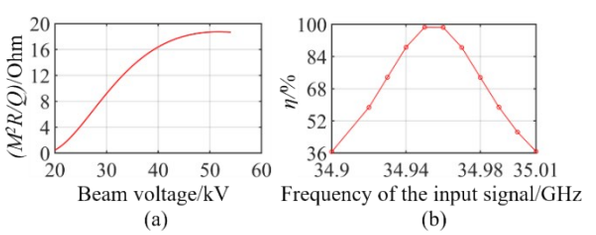

Fig. 5　(a) The effect of M^2R/Q on the beam voltage, and (b) the effect of the absorption efficiency η on the frequency of the input signal of the input cavity loaded by the two beams with the voltage of 45 kV and each current of 5.6 A
图5　(a)M^2R/Q对电子束电压的影响,和(b)在电压45 kV、每个束电流5.6 A的两电子束加载条件下吸收效率η对输入腔输入信号频率的影响

trons passing through the cavity gap are therefore effectively modulated.

More importantly, the Ka-band input cavity needs sufficient beam loading to lower its quality factor (Q). For an ideal input cavity, the input RF power should be consumed by the electrons and the ohmic loss, which can be characterized by the beam loaded quality factor (Q_b), and the ohmic quality factor (Q_0). The total ideal loss of the input cavity is represented by the total quality factor (Q_a), which can be obtained by

$$\frac{1}{Q_a}=\frac{1}{Q_{b1}}+\frac{1}{Q_{b2}}+\frac{1}{Q_0} \quad , \quad (1)$$

where Q_{b1} and Q_{b2} is the beam-1 loaded quality factor and the beam-2 loaded quality factor, respectively. According to the calculation method reported in Ref. [22] and Eq. (1), the effect of the perveance on Q_a is obtained and shown with the red line in Fig. 3. As the perveance increases, Q_a is decreased. A relatively low Q_a is expected in the design, however, corresponding to a large perveance. This is unfavorable for the effective beam wave interaction. So the perveance of ~0.6 μP is selected when taking the balance between the perveance and Q_a into consideration, as well as a large M^2R/Q.

Accordingly, the two beams with the voltage of 45 kV, and every beam current of 5.6 A are used to load the input cavity. The external quality factor (Q_e), is optimized to obtain the optimal matching between the beams and the input cavity [22]. Q_e is selected as 315 by adjusting the coupling structure of the input cavity. When the input cavity is loaded by the two beams, the effect of the absorption efficiency η, which is defined by the ratio of the RF power absorbed by the input cavity with two beams to the input RF power, at the frequency of the input signal is simulated by using the CST software, and shown in Fig. 5(b). When the frequency is 34.96 GHz, η reaches the maximum, which is close to 100 %.

3　Output cavity with two output ports

It should be noted that the power level of 200 kW requires the output cavity and the output waveguide with a high power capacity. So the output cavity is designed with two output ports for sharing the extracted power and accordingly enhancing the power capacity. To balance the effect of two output ports on the field uniformity of the output cavity, we design the output cavity as the model shown in Fig. 2. The central frequency of the output cavity is 34.96 GHz, which is accordance with that of the input cavity.

At Ka-band, a conventional klystron cavity is typically characterized by a high ohmic quality factor (Q_0) and the power extraction from the cavity is closely related to Q_e from the perspective of the cavity circuit. When the stored energy is constant, the integrated-unit cavity distributes the stored energy into three components along the x direction. The ohmic loss is therefore distributed across the enlarged cross section and Q_0 is increased as compared with Q_0 of a conventional single-unit cavity. This allows to design a lower Q_e for efficiently extracting the power from the two ports.

The two output ports produce two Q_es for the output cavity, which can be defined by the external quality fac-

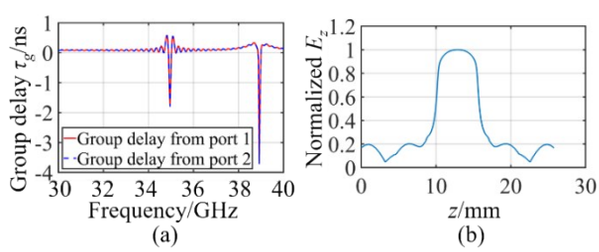

Fig. 6　(a) The group delay τ_g from two output ports, and (b) the absolute amplitude of the normalized E_z field along the axis of the y-direction of the output cavity
图6　(a)两个输出端口的群时延τ_g,和(b)沿输出腔y方向轴线分布的归一化E_z场的幅值绝对值

tor 1 (Q_{e1}), and the external quality factor 2 (Q_{e2}) from port 1 and port 2. The time domain simulation is conducted to obtain the group delay τ_g varying with frequency, as shown in Fig. 6(a). τ_g is the same at the frequency of 34.96 GHz. Q_{e1} and Q_{e2} is correspondingly calculated to be the same value of 98. Figure 6(b) shows the absolute amplitude of the normalized E_z field along the axis of the y-direction of the output cavity. The two output ports produce symmetrical effects on the E_z field of the output cavity.

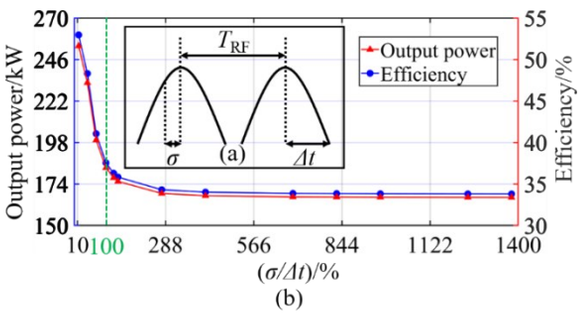

Fig. 7 (a) The shape of a bunch current by the Gaussian model, and (b) the effect of the ratio of the critical parameter σ to Δt, on the output power extracted from the output cavity and the electronic efficiency
图7 (a)高斯模型得到的群聚电流分布形状,和(b)关键参数σ与Δt的比值对输出腔提取的输出功率和电子效率的影响

To examine the capability of extracting power from the two ports, the output cavity is driven by two pre-modulated electron beams equivalently generated by the Gaussian model [9]. Figure 7(a) shows the Gaussian model [23] of the simulated electron bunches. The operating frequency of the output cavity determines the time distance between the adjacent bunches (T_{RF}=1/f). σ and Δt specify the inflection point for the pulse bunch and half of the time width of one bunch, respectively. The ratio, $\sigma/\Delta t$, is the critical parameter of one bunch because it measures the density of clustered electrons. For a constant Δt, a small ratio represents that most electrons are clustered to form a bunch and the bunch current is large in contrast to that of a large ratio. The total charge (q) of one bunch is defined by the product of DC current of one beam and T_{RF}.

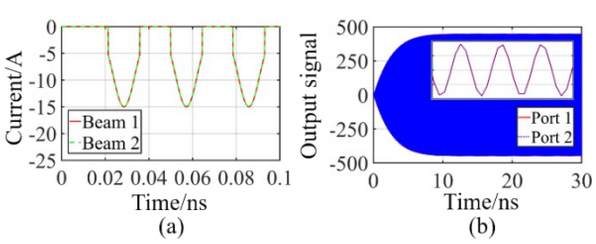

Fig. 8 (a) The waveform of the bunch currents corresponding to the output power of 200 kW (Beam 1 and 2 represent specifically the pre-modulated beam 1 and beam 2), and (b) the output signal obtained from port 1 and 2
图8 (a)对应200 kW输出功率的群聚电流波形(束1和2具体地表示预调制电子束1和电子束2),和(b)从端口1和端口2得到的输出信号

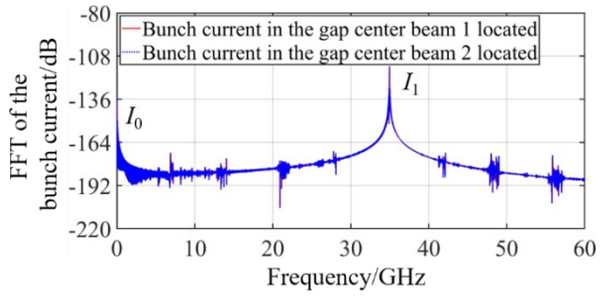

Fig. 9 FFT of the bunch currents in the gap centers beam 1 and beam 2 located (I_0 is the DC current of the beams and I_1 is the current of the fundamental harmonics of the two bunches)
图9 电子束1和电子束2所在间隙中心位置的群聚电流的快速傅里叶变换(I_0是电子束直流电流,I_1是两个群聚块的基波电流)

Figure 7(b) shows the output power and electronic efficiency obtained from the output cavity driven by two pre-modulated electron beams, which are defined by different ratios at constant T_{RF}, Δt, and q. As $\sigma/\Delta t$ is increased, the output power and electronic efficiency are decreased firstly (first stage) and then tend to be saturated (second stage). The power decreases rapidly when $\sigma/\Delta t$ is below 100 %, however, tending into the second stage when the $\sigma/\Delta t$ is larger than 100%. This corresponds to the reduction of the bunch current as $\sigma/\Delta t$ is increased.

When $\sigma/\Delta t$ is 68%, the output cavity can deliver the total peak power of 200 kW, corresponding to the electronic efficiency of ~40%. Every port produces 100 kW. The corresponding shapes of bunch currents of the two pre-modulated beams are the same, as shown in Fig. 8(a). Figure 8(b) shows the output signals from the two ports, which are consistent as shown from the illustration. Figure 9 shows the FFT of the bunch currents in the gap is centered on beam 1 and beam 2 located at the two ports, which is consistent as shown from the illustration. The frequency of I_1 is 34.96 GHz. It is consequently predicted that the designed output cavity with two ports can serve for extracting the required power for the klystron.

4 PIC simulations of the two-beam klystron

According to the design method above, the overall interaction circuit of the klystron has been designed and simulated to demonstrate the effectiveness of the application of the integrated-unit circuits in the Ka-band klystron. The overall circuit consists of the input cavity, buncher cavity 1, buncher cavity 2, and the output cavity, as shown in Fig. 10. The two buncher cavities and the spacing between the adjacent cavities have been optimized to explore the interaction capability of the klystron. Some critical structural parameters are shown in Table 1.

The PIC simulations [23] are conducted when the two electron beams with the voltage of 45 kV and every current of 5.6 A are injected into the overall circuit. The surrounded metal of the klystron is oxygen-free copper

with the conductivity of 5.8×10^7 S/m in the constant magnetic field of 0.8 T used to confine the two beams. The frequency of the input signal is 34.96 GHz. After the beam-wave interaction tends to be stable, the E_z field distribution of the overall circuit is shown in Fig. 10.

Table 1　Some critical parameters
表1　一些关键参数

Structural parameters	Input cavity	Output cavity
Gap width (size along z direction)	0.9 mm	0.7 mm
Height of the coupling cavity (size along y direction)	1.4 mm	1.4 mm
Length of the coupling cavity (size along x direction)	4.7 mm	4.7 mm
Width of the coupling cavity (size along z direction)	1.7 mm	1.5 mm

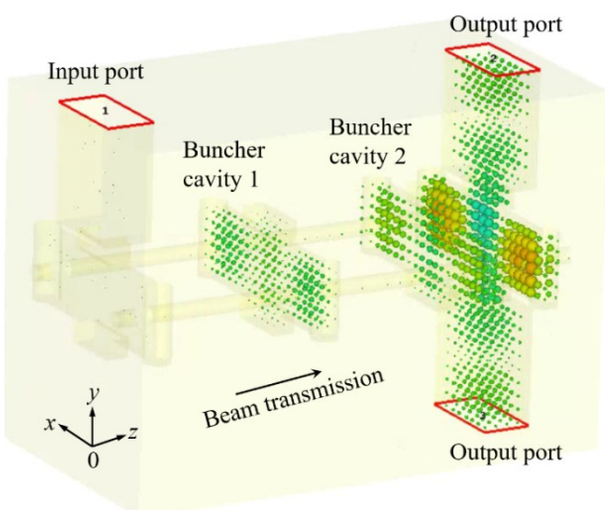

Fig. 10　The overall interaction circuit of the designed klystron with the E_z field
图10　具有E_z场分布的所设计速调管的整体互作用电路

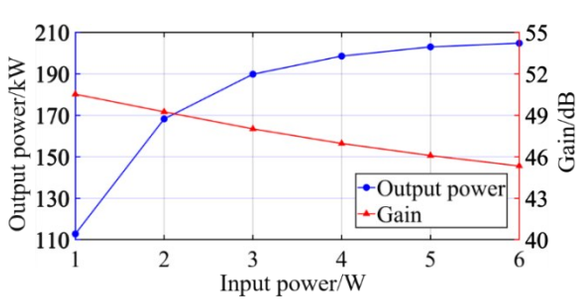

Fig. 11　The effect of the input power on the output power and the gain of the klystron
图11　输入功率对速调管输出功率和增益的影响

Figure 11 shows the effect of the input power on the output power and gain. When the input power (the input frequency is 34.96 GHz) is increased to up to 4 W, the output power of 200 kW and above is obtained and the corresponding gain is 47 dB. The output power is increased as the input power is increased, however, the gain is decreased. When the input power is 5 W, the effect of the frequency of the input signal on the output power and electronic efficiency is obtained, as shown in Fig. 12. The maximum output power of 202.9 kW corresponding to the maximum efficiency of 40.2% has been obtained. The -3-dB bandwidth (-3 dB BW) is 70 MHz.

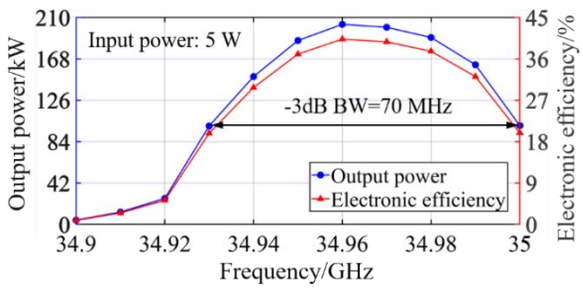

Fig. 12　The effect of the frequency of the input signal on the output power and the electronic efficiency of the klystron
图12　输入信号频率对速调管输出功率和电子效率的影响

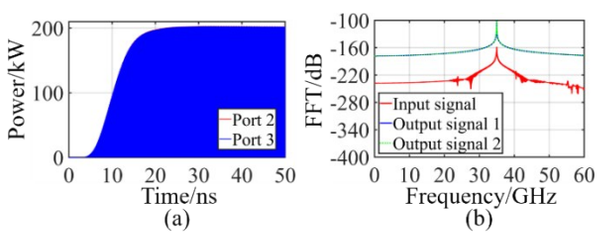

Fig. 13　(a) The output power versus time, (b) the FFT amplitude of the input signal, and output signals from port 2 and port 3 (Output signal 1 and 2 are extracted from port 2 and port 3)
图13　(a)输出功率随时间变化图,(b)输入信号和端口2、3的输出信号的快速傅里叶变换幅值(从端口2和端口3提取得到输出信号1和2)

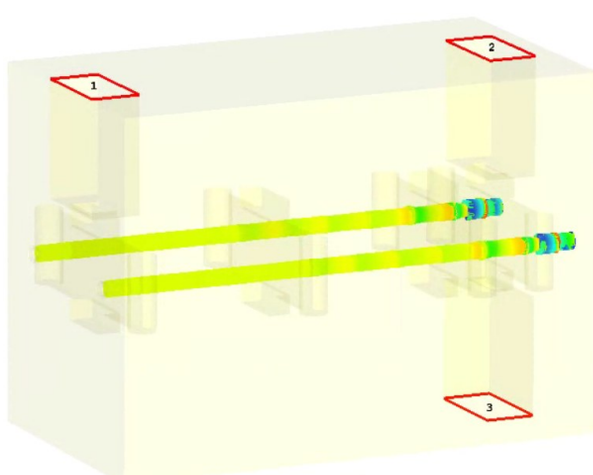

Fig. 14　The beam trajectories
图14　电子束轨迹图

When the frequency and power of the input signal are 34.96 GHz and 5 W respectively, the average output power obtained from every port is 100 kW and the output frequency is 34.96 GHz, as shown in Fig. 13. The total power is 200 kW. The output signals from two ports show the same change as the simulation time goes within 50

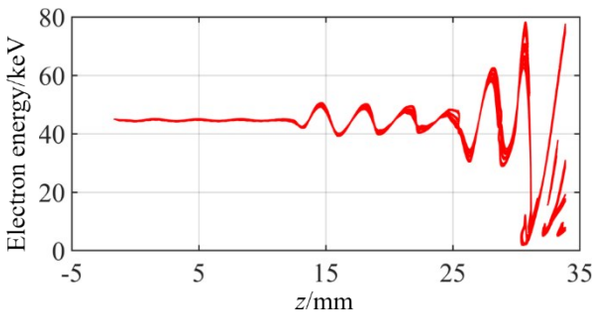

Fig. 15 The phase space of the electrons
图15 电子的相空间图

ns. The frequencies of the input and output signal are the same. Figure 14 shows the beam trajectories after the interaction is stable. Figure 15 shows the phase space of the electrons, which demonstrates the effective energy exchange between the electrons and the overall circuit.

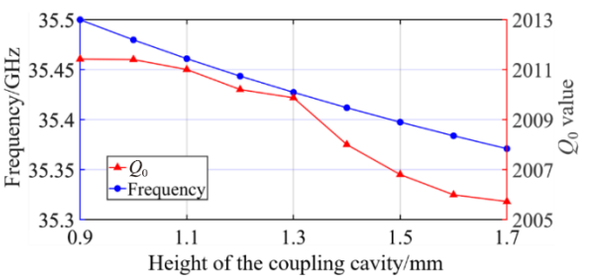

Fig. 16 The effect of the height of the coupling cavity on the frequency and Q_0 value of the buncher cavity
图16 耦合腔高度对群聚腔频率和Q_0的影响

It should be noted that the frequency tuning of buncher cavity 1 and 2 is very important to achieve the efficient operation and bandwidth for the klystron in practice. The efficient integration of the two interaction units largely depends on the energy and distribution pattern of the E_z field across the $\lambda_{g1}/2$ of the cross section. The coupling cavities distributed on both sides of the $\lambda_{g1}/2$ section offer the opportunity for mechanical tuning. One of the two ends along the y-direction of the buncher cavities can be replaced by a piston, which is designed to adjust the height of the coupling cavity. Accordingly, the frequency of the buncher cavities can be tuned to compensate the frequency shift caused by fabrication errors. Figure 16 shows the frequency shift and the variation of Q_0 value caused by the height of one of the two coupling cavities of the buncher cavity.

5 Discussion and conclusion

In this paper, an integrated-unit resonant circuit is proposed to support the efficient beam-wave interaction of a Ka-band klystron for producing 200-kW peak power in the design level and simulation domain, which is a breakthrough power level for Ka-band klystrons nowadays. Two or several typical single beam-wave interaction units, each of which is usually used in conventional klystrons, are integrated to form a new resonant circuit based on the distributed field distribution across the cascaded cross section. Two units have been focused on the design of the input cavity and output cavity with two output ports. The input signal with constant power at ~35 GHz can be absorbed by the input cavity with an absorption efficiency of almost 100%. The output cavity has shown its great potential in producing 200-kW peak power. Finally, the overall interaction circuit of a Ka-band klystron has been designed and simulated to show an effective interaction capability for producing 202.9-kW peak power with the electronic efficiency of 40.2% and the maximum gain of 47 dB.

This paper has focused on the basic designs of the interaction circuit of the Ka-band klystron. The basic integrated-unit circuit has been demonstrated to be efficient for supporting such a klystron with high peak power from the simulation domain. To increase the gain and power capacity, the extended interaction technology may be used in future.

References

[1] CARYOTAKIS G. The Klystron: A Microwave Source of Surprising Range and Endurance [J]. *Physics of Plasmas*, 1998, **5**(5): 1590-1598.
[2] BOOSKE J H. Plasma Physics and Related Challenges of Millimeter-Wave-to-Terahertz and High Power Microwave Generation [J]. *Physics of Plasmas*. 2008, **15**(5): 055502.
[3] BENFORD J, SWEGLE J, Schamiloglu E. High Power Microwaves (3rd Ed.) [M], Boca Raton, FL, CRC Press, 2015.
[4] BERRY D, DENG H, DOBBS R, *et al*. Practical Aspects of EIK Technology [J]. *IEEE Transactions on Electron Devices*. 2014, **61**(6): 1830-1835.
[5] SHIN Y M, PARK G S, SCHEITRUM G P, *et al*. Circuit Analysis of Ka-band Extended Interaction Klystron [C]. In IEEE International Conference on Vacuum Electronics, Seoul, Korea (South) 2003, 108-109.
[6] ZHAO D, GU W, HOU X W, *et al*. Demonstration of a High-Power Ka-Band Extended Interaction Klystron [J]. *IEEE Transactions on Electron Devices*, 2020, **67**(9): 3788-3794.
[7] ZHU F, ZHANG C Q, ZHAO D, *et al*. A 35 GHz 100kW Klystron Amplifier Design [C]. In 2019 44th International Conference on Infrared, Millimeter, and Terahertz Waves (IRMMW-THz), Paris, France, 2019, pp. 1-2.
[8] WANG H, XUE Q Z, ZHAO D, *et al*. A Wideband Double-Sheet-Beam Extended Interaction Klystron with Ridge-Loaded Structure [J]. *IEEE Transactions on Plasma Science*, 2011, **39**(3): 1796-1802.
[9] ZHANG C Q, LV S Y, CAI J, *et al*. Exploration of a Kilowatt-Level Terahertz Amplifier Based on Higher-Order Mode Interaction [J]. *IEEE Transactions on Electron Devices*, 2022, **69**(9): 5223-5228.
[10] LIU W X, LI K, GAO P, *et al*. Nonlinear Theory for Beam-Wave Interactions of Two Electron Beams with Higher Order TE20 Mode in Serpentine Waveguide Traveling Wave Amplifier [J]. *Physics of Plasmas*, 2018, **25**(12): 123106.
[11] XU C, MENG L, HU C F, *et al*. Analysis of Dual-Frequency Radiation from a G-band Extended Interaction Oscillator with Double Sheet Electron Beam [J]. *IEEE Transactions on Electron Devices*, 2019, **66**(7): 3184-3189.
[12] TIAN Y Y, SHU G X, GONG Y B, *et al*. A Novel Slow-Wave Structure-Coupled Double Folded Waveguide Operating at High-Order TM_{20} Mode for Terahertz TWT [J]. *IEEE Electron Device Letters*, 2021, **42**(12): 1871-1874.
[13] LI S F, HUANG H, DUAN Z Y, *et al*. Demonstration of a Ka-Band Oversized Coaxial Multi-Beam Relativistic Klystron Amplifier for High Power Millimeter-Wave Radiation [J]. *IEEE Electron Device Letters*, 2022, **43**(1): 131-134.
[14] ZHANG X, ZHANG R, WANG Y. Study of a Dual-Mode Multibeam Interaction Circuit with Coaxial Structure for Ka-Band High-Power

EIK [J]. *IEEE Transactions on Electron Devices*, 2021, **68**(2): 822-828.
[15] ZHANG X, ZHANG R, WANG Y. Research on a High-Order Mode Multibeam Extended Interaction Oscillator with Coaxial Structure [J]. *IEEE Transactions on Plasma Science*, 2020, **48**(6): 1902-1909.
[16] YIN Y, ZENG F B, WANG B, *et al*. Preliminary Study of a Multiple-Beam Extended Interaction Oscillator with Coaxial Structure [J]. *IEEE Transactions on Electron Devices*, 2018, **65**(6): 2108-2113.
[17] YIN Y, BI L J, WANG B, *et al*. Preliminary Circuit Analysis of a W-Band High Power Extended Interaction Oscillator with Distributed Hollow Electron Beam [J]. *IEEE Transactions on Electron Devices*, 2019, **66**(7): 3190-3195.
[18] LIN F M, WU S N, XIAO Y J, *et al*. A 0.3 THz Multi-Beam Extended Interaction Klystron Based on $TM_{10,1,0}$ Mode Coaxial Coupled Cavity [J]. *IEEE Access*, 2020, **8**(12): 214383-214391.
[19] BI L J, YIN Y, WANG B, *et al*. Tractable Resonant Circuit with Two Nonuniform Beams for a High-Power 0.22-THz Extended Interaction Oscillator [J]. *IEEE Electron Device Letters*, 2021, **42**(6): 931-934.
[20] BI L J, JIANG X Y, QIN Y, *et al*. Power Enhancement of Sub-Terahertz Extended Interaction Oscillator Based on Overmoded Multi-Gap Circuit and Linearly Distributed Two Electron Beams [J]. *IEEE Transactions on Electron Devices*, 2022, **69**(2): 792-797.
[21] BI L J, QIN Y, XU C, *et al*. Design and Analysis of an Overmoded Circuit for Two-Beam Sub-THz Extended Interaction Oscillator [J]. *IEEE Transactions on Electron Devices*, 2021, **68**(11): 5807-5813.
[22] JIANG X Y, BI L J, QIN Y, *et al*. Study of the Input Cavity Characteristics with Two-Beam Loading for Developing a Compact and High-Power Ka-Band Klystron [J]. *IEEE Transactions on Electron Devices*, 2022, **69**(10): 5852-5857.
[23] CST Microwave Studio, CST, Darmstadt, Germany, 2014.